Renewable Energy 35 (2010) 2867–2873

Contents lists available at ScienceDirect

Renewable Energy

journal homepage: www.elsevier.com/locate/renene

Solar variability of four sites across the state of Colorado

Matthew Lave, Jan Kleissl*

Dept. of Mechanical & Aerospace Eng., University of California, San Diego, 9500 Gilman Drive, La Jolla, CA 92093-0411, USA

ARTICLE INFO

Article history:
Received 10 November 2009
Accepted 7 May 2010
Available online 7 June 2010

Keywords:
Coherence
Grid-connected PV systems
Solar variability
Photovoltaic
Spectral analysis

ABSTRACT

Solar Global Horizontal Irradiance (GHI) fluctuates on both short (seconds to hours) and long (days to months) timescales leading to variability of power produced by solar photovoltaic (PV) systems. Under a high PV penetration scenario, fluctuations on short time scales may require a supplementary spinning power source that can be ramped quickly, adding significant external cost to PV operation. In order to examine the smoothing effect of geographically distributed PV sites, GHI timeseries at 5 min resolution at four sites across the state of Colorado were analyzed. GHI at the four sites was found to be correlated due to synchronous changes in the solar zenith angle. However, coherence analysis showed that the sites became uncorrelated on time scales shorter than 3 h, resulting in smoother average output at short time scales. Likewise, extreme ramp rates were eliminated and the spread in ramp rate magnitude was significantly reduced when all four sites were averaged. Nevertheless, even for the averaged output, high frequency fluctuations in PV power output are relatively larger in magnitude than fluctuations expected from wind turbines. Our results allow estimation of the ancillary services required to operate distributed PV sites.

1. Introduction

Over the past few years, there has been an increasing interest in harnessing renewable energy sources such as wind and solar power as a supplement to, or replacement for, current carbon-based power sources. However, at high grid penetration, variability of these renewable sources has the potential to affect grid reliability and energy cost. Wind power has thus far been the more popular technology for large-scale implementation, with about 121 GW of wind power installed across the world at the end of 2008 [1]. In areas where a large percentage of the power is provided by wind, fast-ramping of other power sources has been used to counteract wind variability [2].

In comparison to wind power, installed solar photovoltaic (PV) power capacity was relatively small, with only about 13 GW at the end of 2008 [1]. However, PV installation has increased rapidly over the past few years. Since 2002, PV power capacity has increased 48% per year, on average, and is expected to continue to be the fastest growing energy technology in the world [3]. Since PV is growing so quickly, it is pertinent to study high-penetration scenarios.

Geographically dispersing wind power sites is an effective way of reducing wind variability, as power production at different sites typically becomes uncorrelated over a few 100 km [4–6]. In Northern Europe wind power supply from sites more than 1500 km apart is uncorrelated [7]. When aggregated, the output of 1496 widely spread wind turbines in Germany showed maximum variations of 60% in 4 h. Similarly, one would expect that geographic dispersion of solar energy production sites could mitigate solar variability caused by atmospheric transmissivity changes in short timescales (clouds), while being largely ineffective in mitigation of the day-night-solar variability.

Analyzing a month of 1 min radiation data from 11 sites over 75 × 75 km in Wisconsin (a mid-latitude frontal weather regime), Long and Ackerman (1995) determined the correlation of Global Horizontal Irradiance (GHI) and GHI normalized by clear sky radiation [8]. As expected, the correlation coefficients were smaller for the normalized value, as the synchronized occurrence of rising and setting sun at all stations contributes significantly to a high correlation. Large day-to-day differences in correlations were observed indicating limitations for average statistics in describing or modeling insolation. Moreover, for individual days – especially overcast days – there was significant scatter in the correlation versus distance plots for all stations pairs indicating that atmospheric transmissivity is not an isotropic process. Barnett et al. (1998) used Oklahoma Mesonet data from 111 GHI sensors to define spatial correlograms [9]. Subtracting out the diurnal signal, they found that characteristic length and time scales (i.e. the distances and time differences at which correlation goes to zero) were

* Corresponding author.
E-mail address: jkleissl@ucsd.edu (J. Kleissl).

0960-1481/$ – see front matter © 2010 Elsevier Ltd. All rights reserved.
doi:10.1016/j.renene.2010.05.013

300 km and 60 min, respectively. Curtright and Apt (2008) examined three PV sites spread across hundreds of kilometers in the state of Arizona and found a reduction in average 10 min step size magnitude and in standard deviation for the sum of all three sites [10]. However, they also found that short timescale variability of large-scale PV power was still significant and that the geographical diversity did not dampen PV variability enough to eliminate the need for substantial supplemental power sources. Wiemken et al. (2001) studied 100 PV systems spread across Germany, and also found a decrease in average step size magnitude and standard deviation for the sum of all systems, but did not present timescale variability analysis [11].

In this paper we study the variability of measured GHI at four different sites across the state of Colorado. This choice is motivated by the fact that the greatest spatial density of 1–5 min resolution irradiance data exists in Colorado. Topographical and meteorological differences between Wisconsin, Oklahoma, Arizona and Colorado also warrant the analysis of variability over different regions. The sharper terrain difference across these Colorado sites may lead to more varied weather patterns and increased geographic variation. Moreover, we extend the existing literature by analyzing shorter time scales (5 min) and examining coherence between the sites and its effect on smoothing average output at different time scales through spectral analysis.

2. Data

While ultimately PV array power output is the relevant variable for variability analysis, 90% of the variability in PV output is explained by variability in GHI. Consequently, here we assume that solar radiation is proportional to PV power output and we use radiant flux density (W m^{-2}) rather than power for this analysis, neglecting the influence of PV panel temperature on panel efficiency. Furthermore, while variability analysis of PV output is more practically relevant, these studies are not as representative, since they depend on the system specifications, and there is generally less publicly available time-resolved data for PV output.

GHI data were obtained from the National Renewable Energy Laboratory's (NREL) Measurement and Instrumentation Data Center (MIDC) [12]. Sites were chosen which were within a few hundred kilometers of one another such that they would typically feed into one utility grid, and had complete data for Jan 1, 2008–Dec 31, 2008. Four sites fit these criteria: the National Wind Technology Center (NWTC), the NREL Solar Radiation Research Laboratory (SRRL), the South Park Mountain Data (SPMD), and the Xcel Energy Comache Station (XCEL, Fig. 1). The distances between sites are shown in Table 1. The NWTC site has an Eppley Laboratory, Inc. Precision Spectral Pyranometer, SRRL data were collected using a Kipp and Zonen CMP 22 pyranometer, and the XCEL site uses a LICOR LI-200 silicon pyranometer. All sites had data at 1 min resolution except for SPMD where a LI-200 was operated at 5 min temporal resolution.

Although a greater geographical wealth of solar radiation data is available through NREL's National Solar Radiation Database (NSRDB), these data are only recorded once per hour, and much of it is not based on GHI measurements. Using 1 h resolution, even if it is an average of data collected at shorter intervals, will filter out the shorter time-scale variability that produce the largest ramp rates (RRs). For example, large RRs caused by clouds occur on scales of seconds to 10 min. Fig. 2 illustrates the difference in RRs between hourly data and 1 or 5 min data, which is the motivation for using the unique collocation of highly time-resolved data in Colorado in this paper.

Visual examination of the timeseries revealed that SPMD tends to be shaded in the morning due to high surrounding terrain. This

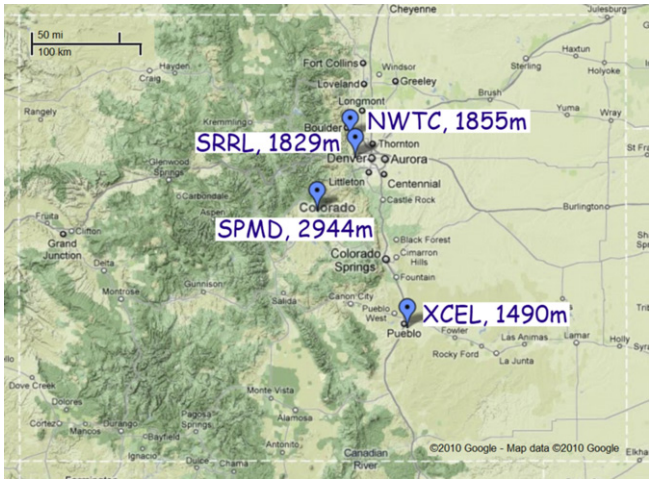

Fig. 1. The sites used for this study on a terrain map with elevations in meters: National Wind Technology Center (NWTC), Solar Radiation Research Laboratory (SRRL), South Park Mountain Data (SPMD), and Xcel Energy Comanche Station (XCEL). Map © 2010 Google - Map Data © 2010 Google.

variability is naturally occurring (i.e. it would be the same for a PV array at the same site), but was eliminated from the dataset by filtering out data at large solar zenith angles (SZAs). We also found that NWTC seems to be shaded at several times of the day, especially around 1400 MST. This unexplained shading in NWTC was difficult to correct for and the realization of the shading will be further discussed in the results section.

3. Methods

3.1. Data quality control

Since this paper does not attempt an assessment of the mean solar resource, but an analysis of the variability in GHI, slight sensor differences in offset and/or gain will not have a significant effect on our results. Nevertheless, we calibrated the sites against each other on clear days in the region, when they are expected to be similar given the small variability of atmospheric composition over short distances. The SRRL site is maintained daily by trained NREL staff and is considered to have the best data. Therefore, the NWTC and XCEL data were corrected using a linear regression against SRRL on nine clear days (Jan 13, Mar 3, Apr 14, Jun 14, Jul 13, Aug 28, Sep 16, Nov 19, Dec 25). The SPMD site was not corrected since higher clear sky atmospheric transmissivity associated with its high elevation (expected transmissivity of about 81% versus 79% for the other sites) would result in a different clear sky GHI.

A linear regression of GHI(SRRL) = A GHI(site X) + B was applied. The regression constants A and B for the XCEL site were nearly constant throughout the year, so an overall linear fit of all nine clear days was applied. The regression constants for NWTC showed a seasonal variation. Consequently, interpolated (time dependent) slopes and intercepts based on regressions from the nine clear days

Table 1
Distance between sites.

From	To	Distance
NWTC	SRRL	19 km
NWTC	SPMD	78 km
NWTC	XCEL	197 km
SRRL	SPMD	65 km
SRRL	XCEL	178 km
SPMD	XCEL	149 km

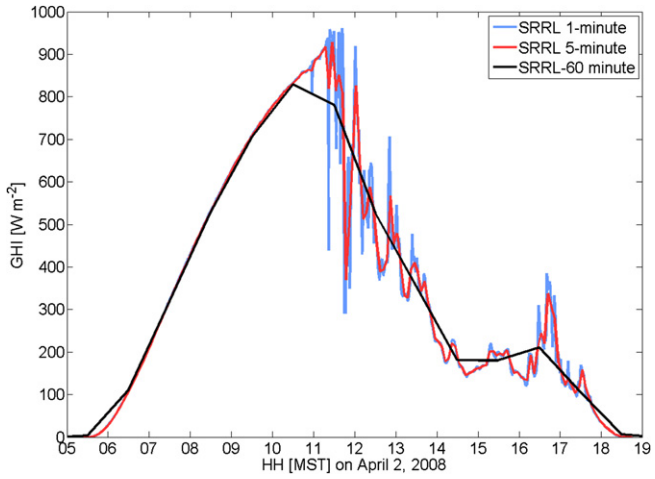

Fig. 2. Comparison of original 1 min GHI data, with 5 min and 60 min averages for SRRL on April 2, 2008.

were used. The variability in the regression coefficients is an indication of differences in the cosine response of the sensors or of a sensor that is not leveled properly. While this will affect the average and seasonality of the mean solar resource, it has little influence on short-term RRs analyzed in this study.

The largest intercept from all regressions was $B = 59.79\ \mathrm{W\,m^{-2}}$, so all GHI less than 60 $\mathrm{W\,m^{-2}}$ were eliminated in the dataset. In this way, data near sunrise and sunset, which are prone to topographic shading effects and have little relevance in practice since power output is small and large RRs do not occur, are removed from the dataset. We stress that more advanced corrections (such as dependent on SZA) could be applied, but natural variability in air-mass between sites and the objective of quantifying *variability* means the added value of such corrections is small.

3.2. Spatial and temporal correlation

To test the smoothing effect of geographic dispersion, a fifth virtual site, called average (AVG4), was defined as the average GHI of all four sites. Due to SPMD only having 5 min temporal resolution, the average is comprised of the 5 min averages of NWTC, SRRL, and XCEL, combined with the SPMD data.

For utilities and independent system operators, frequency of occurrence and magnitude of RRs of renewable power sources are the critical quantity of interest. A probability distribution function (pdf) can be used to compare the probabilities of different RR for the individual sites and for the average of all four sites. Five minute, daytime only (defined as GHI greater than 60 $\mathrm{W\,m^{-2}}$) data were used for all sites. Ramps occur naturally throughout the day with changes in the SZA. However, since these ramps are predictable they are of lesser concern and were removed from the analysis. Expected clear-sky irradiance (SKC) was calculated using standard astronomical formulae and assuming that clear sky atmospheric transmissivity is $(0.75 + 2 \times 10^{-5}\ \mathrm{m^{-1}} \times \mathrm{Z})$, where Z is station elevation in meters. SKC was subtracted from the GHI at each site, such that the remaining value was variation from expected irradiance. The RRs of these variations were calculated as the difference between successive data points over 5 min, using the equation $\mathrm{RR} = [\mathrm{GHI(t)} - \mathrm{SKC(t)} - \mathrm{GHI(t\text{-}5\ min)} + \mathrm{SKC(t\text{-}5\ min)}]/5\ \mathrm{min}$, given in units of $\mathrm{W\,m^{-2}\,min^{-1}}$.

Power Spectral Density (PSD) analysis provides insight into how much of the variability in GHI can be explained by events at different frequencies such as daily and seasonal cycles in SZA, as well as variations in atmospheric transmissivity due to meteorological events such as cloud cover which occur over a range of frequencies. PSD analysis gives an indication of the amount of complementary ancillary services necessary to counteract vairability at different frequencies. The larger the PSD, the larger the variance in power output and the larger the required rampable (conventional) power sources to make up for the difference. Low frequency oscillations, which may be due to daily or even seasonal cycles, can be supplemented with rather constant power sources such as traditional large power plants. High frequency oscillations are more challenging and must be supplemented with faster ramping power sources.

To test for overall correlation the Pearson correlation coefficient was calculated between the GHI timeseries at different sites. Due to the synchronized SZA variations at different sites in the same region, the correlation coefficients are usually close to one. Nevertheless, the smaller the correlation coefficient, the more smoothing would be expected (a correlation coefficient of −1 would indicate perfect smoothing of the aggregate power output of two sites). A better measure for correlation on shorter timescales, which is more important for smoothing the extreme ramp rates, is the coherence spectrum [13]. The coherence spectrum provides a normalized covariance at each frequency, allowing analysis of correlation at short timescales. Since long timescales (seasonal cycles, synoptic weather patterns, and daily cycles) affect all sites in the same way, the coherence spectrum between any two sites is expected to have a value close to 1. On shorter timescales, the coherence spectrum indicates how correlated intra-day events such as transient clouds or mesoscale weather systems are between two sites. The timescale at which sites become uncorrelated is an indication of the longest timescale on which they will dampen aggregate vairability.

4. Results

4.1. Ramp rates

In the tables and figures referenced in this section the values for AVG4 are given throughout. However, we will wait to discuss these in a coherent fashion at the end of this section. The average and maxima of the magnitude of RRs for each site are shown in Table 2. With an average RR magnitude of 9.9 $\mathrm{W\,m^{-2}\,min^{-1}}$ SPMD had the largest, while XCEL had the smallest at 6.2 $\mathrm{W\,m^{-2}\,min^{-1}}$. The maximum RRs are very similar for all sites. Since the mean absolute value of the RR is already a measure of the RR variability, the standard deviation of the RR (not the absolute value) is expected to give qualitatively similar results as is confirmed in Table 2. However, the kurtosis (the 4th moment normalized by the 2nd moment squared) weights extreme RR events higher. The fact that SPMD had the smallest kurtosis and largest standard deviation suggests that medium sized RRs were common, but extreme RRs were rarer than at the other three sites. The XCEL site had the lowest standard deviation but the highest kurtosis. Sensor shading would produce more extreme RRs, so the fact that the NWTC kurtosis is similar to SRRL and the standard deviations were equal

Table 2
Five minute ramp rate statistics for daytime GHI in 2008.

	Mean(|RR|) [$\mathrm{W\,m^{-2}\,min^{-1}}$]	Max(|RR|) [$\mathrm{W\,m^{-2}\,min^{-1}}$]	Std(RR) [$\mathrm{W\,m^{-2}\,min^{-1}}$]	Kurtosis(RR) [-]
NWTC	7.4	178.6	16.8	21.3
SRRL	7.4	160.8	16.8	20.6
SPMD	9.9	188.6	21.8	17.7
XCEL	6.2	163.7	14.9	23.8
AVG4	5.6	111.8	10.8	15.4

indicates that shading likely was not a significant contributor to the variability at the site. Generally the kurtosis is much larger than 3 (the value expected for a Gaussian distribution) indicating the prevalence of extreme events (or large RR) in the distribution.

The probability density (pdf) of RRs is shown in Fig. 3. Consistent with the standard deviations found previously, the pdf of SPMD is the widest, indicating higher probabilities of large RRs. The XCEL site has the most narrow pdf, meaning it is the least likely to have a large RR.

The cumulative density (cdf) of the absolute value of RR for each site is shown in Fig. 4. From the cdf, one can read the probability of RRs larger than a threshold. For the XCEL site, there is a 5% chance that RRs will be larger in magnitude than 31 W m^{-2} min^{-1}. At both NWTC and SRRL, there is a 5% chance of a RR with magnitude 36 W m^{-2} min^{-1} or larger. Again, SPMD shows the highest propensity to large RRs. There is a 5% chance that a RR at SPMD is larger than 49 W m^{-2} min^{-1} in magnitude. Given our 5 min time-step and an average length of day of 10.7 h, an event with a 5% chance occurs on average about 6 times per day.

4.2. Power spectral analysis

The power spectrum for all sites calculated for the entire year 2008 is shown in Fig. 5. In all four spectra, the largest peak appears at a frequency of 1.16×10^{-5} Hz, which corresponds to a period of 24 h. This is expected due to cyclic daily availability of the SZA. Longer period cycles corresponding to variability over days to months also show a large PSD due to weather patterns and the seasonal variability of the SZA [10]. The higher frequency ($f > 2 \times 10^{-3}$ Hz) variations are dominated by atmospheric transmissivity changes by clouds. Generally, the PSD decreases with increasing frequency, but the rate of decrease varies from site to site.

To quantify this decrease in variability as a function of frequency at each site, linear fits for periods of less than 1 h, 1–3 h, and 3–11 h are shown in Table 3. The SRRL site consistently had a steeper slope compared to the other sites. For periods less than 1 h, the slopes ranged from −1.559 (SRRL) to −1.392 (SPMD). At 1–3 h, SRRL again had the steepest slope of −1.477, but all the others had flatter slopes than for periods less than 1 h. For 3–11 h, the SRRL, NWTC, and XCEL slopes were −1.432, −1.452, and −1.509, respectively, but the SPMD slope was even flatter than in the other period ranges, at only −0.981. The ratios of the integrals of the PSD over periods shorter than 1 h to the total integral over all periods (i.e., the fractions of total variance contained in the high frequencies) are also shown in Table 3 (2nd to last column). XCEL had the smallest ratio of high frequency oscillations, which suggests it has relatively more variability on long time scales. NWTC and SRRL had smaller integral ratios than SPMD, suggesting more high frequency forcing such as clouds at SPMD than at the other sites. This is also consistent with the flatter slope at SPMD for $f > 1/3$ h^{-1} and the width of the pdf in Fig. 3.

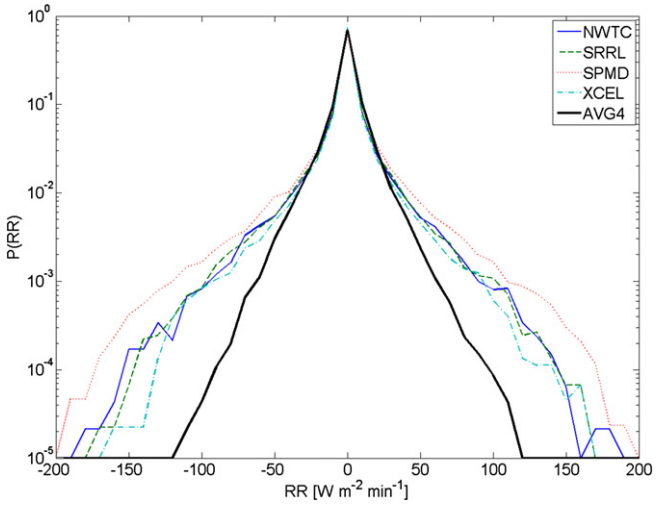

Fig. 3. Probability density function (pdf) of the ramp rate of NWTC, SRRL, SPMD, XCEL sites and the average of all four sites (AVG4) for 5 min GHI-SKC data.

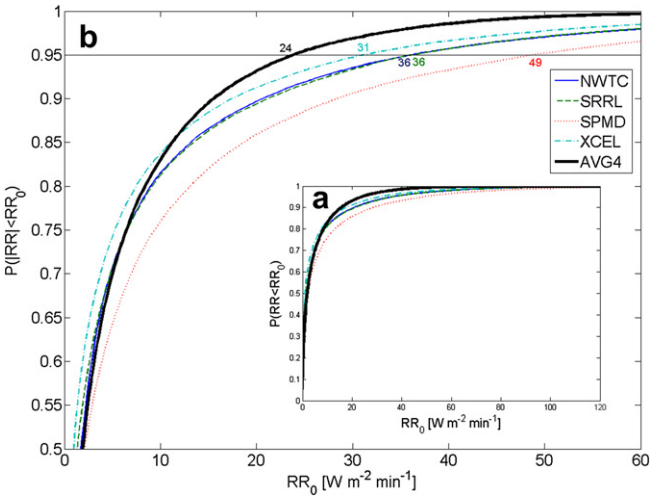

Fig. 4. Cumulative probability distribution function (cdf) of the absolute value of GHI-SKC ramp rate over 5 min for NWTC, SRRL, SPMD, XCEL and their average. (a) Entire cdf; (b) Zoom in to the 'knee' of the graph showing the probability of medium to large RRs. The black horizontal line shows $P = 0.95$ and intersects with this line are labeled with the RR magnitude which is exceeded 5% of the time.

4.3. Correlation coefficients and coherence spectrum

After discussing variability at each site, we will now compare the sites to one another to see if geographic dispersion can mitigate solar variability. The Pearson correlation of GHI and GHI-SKC at each of the sites increases with geographic proximity of the sites (Table 4). NWTC and SRRL show the strongest correlation due to their geographical proximity. The XCEL and SPMD sites show smaller correlations to the other two sites probably due to their large geographic distance (XCEL) and higher altitude (SPMD). Mountain ranges may act as natural barriers to cloud motion. GHI-SKC indicates the deviation of GHI from an expected value (SKC), so correlation of GHI-SKC is a better measure of ability to dampen variability on short time scales. As seasonal and diurnal cycles are taken out, the correlation coefficients for GHI-SKC decrease substantially (especially for distant sites) and become similar to the coherence at small time scales (Fig. 6). The weaker correlation of XCEL and SPMD to the other sites implies that integrating the XCEL and SPMD sites into the same grid as SRRL and NWTC will dampen fluctuations in solar power output of the average of all sites.

The coherence of each of the four sites with the other sites is shown in Fig. 6. Generally the correlation between sites is highest for seasonal changes (about 0.8). Then, the correlation decreases with decreasing time scale but remains large including peaks at periods of 24 and 12 h. A reduction in coherence is observed at a period of 2 days, which may indicate a decorrelation due to atmospheric transmissivity differences caused by different weather patterns or aerosol absorption. NWTC and SRRL again show the highest correlation, but only for timescales longer than 3 h. For periods shorter than 12 h (3 h for SRRL-NWTC), all sites have

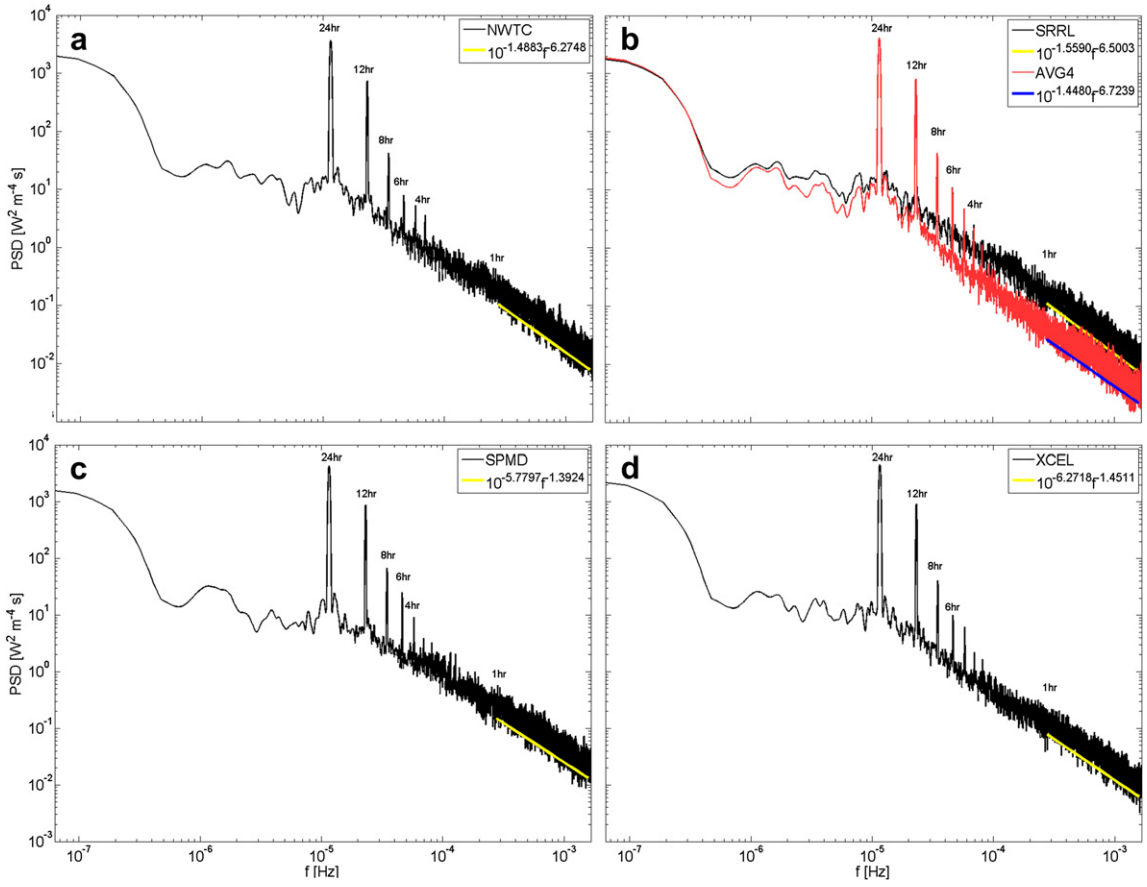

Fig. 5. Power spectral density of (a) NWTC (b) SRRL and AVG4 (c) SPMD, and (d) XCEL for 2008 using 5 min averaged GHI data. The yellow line is the linear best fit line for time scales less than 1 h. (b) The blue line is the linear best fit line for time scales less than 1 h for AVG4.

similar coherences of about 0.2, showing less correlated variation over short time scales. Consequently, when combined, the four sites are expected to smooth the averaged output on time scales shorter than 12 h.

4.4. Averaged output from all sites

The GHI timeseries sample (Fig. 7) showed that while each individual site fluctuates significantly over these two days, the average of all four sites has much smaller fluctuations. This confirms anecdotally that averaging geographically separated sites will lead to a smoother output.

RR analysis of the average site confirms this effect (Table 2). There is a decrease in mean magnitude, maximum magnitude, standard deviation, and kurtosis for the AVG4 site over each of the individual sites. Particularly of note are the standard deviation and kurtosis, suggesting few extreme RRs. Fig. 3 confirms that the tails of the AVG4 pdf go to zero at a lower RR than the individual sites, indicating a lower probability of extreme RRs for AVG4. Based on the AVG4 cdf there was a 5% probability that the magnitude of the RR would be greater than 24 W m^{-2} min^{-1} (Fig. 4). This was less than half the RR found for the SPMD site alone.

While RR analysis has demonstrated a reduction in magnitude of RR of averaged irradiances from four sites, a power spectral analysis allows quantifying the time scales over which most of the reduction in RR occurs (Fig. 5b). The amplitude of the AVG4 PSD was smaller than the SRRL PSD for nearly all time scales. The PSD of AVG4 became visibly smaller than the individual sites for $f > 2 \times 10^{-6}$ Hz (5.8 days) and the ratio (as indicated by the vertical distance on the log scale) became largest and remained constant for $f > 1 \times 10^{-4}$ Hz (2.8 h). This was consistent with the shortest period of high correlation observed for SRRL and NWTC in Fig. 6. Linear best fit lines and integral ratios of the PSD at the AVG4 site had consistent, steep slopes over all three period ranges that were close to the steepest slopes of any of the individual sites, indicating a strong reduction of high-frequency variability for AVG4. It should also be noted that the offset of the linear fit for the AVG4 site was the smallest for all three period ranges, which made the amplitude

Table 3
Statistics on the PSDs in Fig. 5. Columns 2–5 give linear regressions in a log–log plot, where the exponent of f is the slope. Column 6 is the fraction of the total variance contained in time scales less than 1 h. Column 7 is the mean PSD intensity for timescales less than 1 h.

	Linear regression for periods less than 1-h	Linear regression for periods of 1–3 h	Linear regression for periods of 3–11 h	Linear regression for all periods	$(\int_{f>1\text{hr}^{-1}} \text{PSD})/(\int_{\text{all } f} \text{PSD})$	$<\text{PSD} \mid f > 1\text{hr}^{-1}>$ [W^2 m^{-4} s]
NWTC	$10^{-6.275}f^{-1.488}$	$10^{-4.918}f^{-1.115}$	$10^{-6.297}f^{-1.452}$	$10^{-5.857}f^{-1.352}$	0.0244	0.0448
SRRL	$10^{-6.500}f^{-1.559}$	$10^{-6.301}f^{-1.477}$	$10^{-6.186}f^{-1.432}$	$10^{-5.954}f^{-1.380}$	0.0224	0.0437
SPMD	$10^{-5.780}f^{-1.392}$	$10^{-5.323}f^{-1.256}$	$10^{-4.182}f^{-0.981}$	$10^{-5.333}f^{-1.247}$	0.0325	0.0684
XCEL	$10^{-6.272}f^{-1.451}$	$10^{-4.888}f^{-1.057}$	$10^{-6.640}f^{-1.509}$	$10^{-5.896}f^{-1.328}$	0.0160	0.0337
AVG4	$10^{-6.724}f^{-1.448}$	$10^{-6.617}f^{-1.408}$	$10^{-8.002}f^{-1.757}$	$10^{-6.674}f^{-1.432}$	0.0064	0.0117

Table 4
Correlation coefficient between the sites for both GHI and GHI-SKC for daylight hours over the year 2008.

	NWTC		SRRL		SPMD		XCEL	
	GHI	GHI-SKC	GHI	GHI-SKC	GHI	GHI-SKC	GHI	GHI-SKC
NWTC	X	X	0.827	0.636	0.659	0.361	0.706	0.300
SRRL	0.827	0.636	X	X	0.658	0.365	0.706	0.306
SPMD	0.659	0.361	0.658	0.365	X	X	0.658	0.273
XCEL	0.706	0.300	0.706	0.306	0.658	0.273	X	X

of variation of the AVG4 site on short timescales smaller than any of the other sites. For variability at periods shorter than 1 h, the relative variance was less than half the relative variance at XCEL (the site with the least variability) and the mean PSD was less than a third the XCEL mean, indicating a significant decrease in high frequency variability when all four sites were averaged together.

5. Discussion

Overall, a significant smoothing effect was observed when the averaged solar irradiance at four solar sites across Colorado is compared to the individual sites. RR analysis showed a significant decrease in the mean RR magnitude, maximum RR magnitude, standard deviation, and kurtosis of the average compared to each site individually, consistent with previous work [10,11]. Both the pdf and cdf of RRs indicated that the average of all four sites is less likely to have large fluctuations than each of the other sites individually. There was a 23–51% decrease in the RR that has a 5% probability of occurring for AVG4. This will mean smaller RRs and less uncertainty in operating the grid resulting in a reduced need for the procurement of expensive ancillary services or spinning reserve.

The variability of solar radiation over short timescales also decreased significantly for the averaged irradiance. Power spectral density analysis showed an overall slope of $f^{-1.43}$ for the average, while the individual sites ranged from $f^{-1.38}$ to $f^{-1.25}$ These were all consistent with slopes for solar spectra, such as those found by Curtright and Apt of $f^{-1.3}$ for periods down to 10 min. However, these slopes were larger than the Kolmogorov spectrum ($f^{-5/3}$) expected for wind turbines and found by Apt (2007) and others [14]. PSD analysis showed significant decreases in the mean PSD intensity at frequencies corresponding to periods shorter than 1 h and the ratio of high frequency oscillations to all oscillations. This drop-off of high frequency oscillations was consistent with Nanahara et al.'s (2004) findings for distributed wind turbine sites [15]. The average reduced high frequency fluctuations, but did not

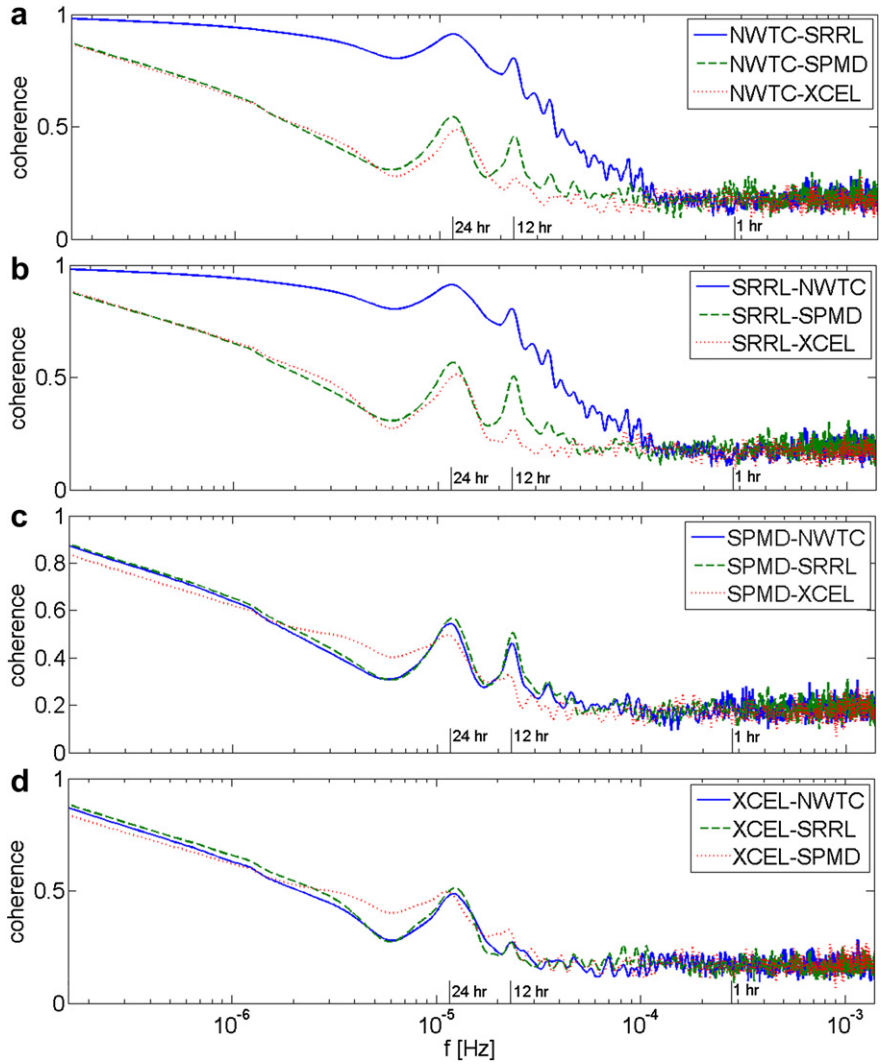

Fig. 6. Coherence spectrum between GHI for each pair of sites for 2008.

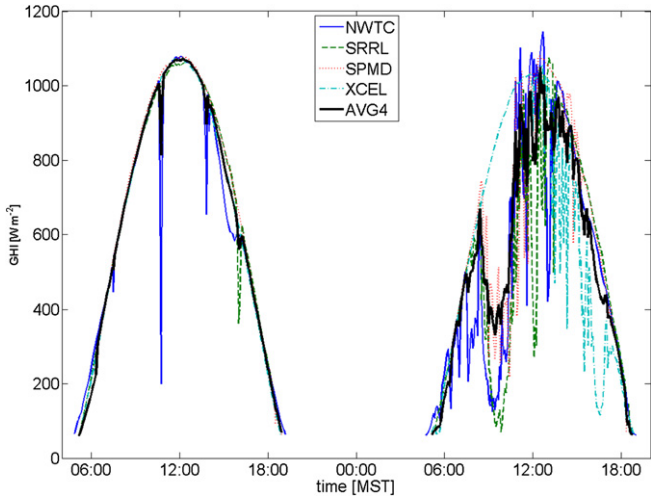

Fig. 7. Five minute GHI data at NWTC, SRRL, SPMD, XCEL and their average over June 10th and 11th, 2008, with values less than 60 W m^{-2} filtered out.

eliminate them. High frequency fluctuations in PV power output could be a problem because they require another power source to change its output at high frequencies in order to compensate.

High frequency variability could be reduced even further by increasing the number of and geographic dispersion between sites. For example, high correlation was found in GHI between NWTC and SRRL which are only 19 km apart. Coherence analysis showed that NWTC and SRRL were highly correlated in GHI for timescales longer than 3 h, but become nearly uncorrelated for timescales less than 3 h. Consequently while variability on large time scales will not decrease significantly by adding more sites, additional sites even if only a few km apart will decrease the short term intermittency.

As PV penetration into electricity grids increases, it is important to consider the intermittency, capacity factors, and peak shaving potential of PV, including the effect energy storage can have on the power output from PV systems. The appendix lists a simple analysis performed for the state of Colorado of the potential of PV to match the load.

Acknowledgements

We thank Tom Stoffel of NREL for his advice on Colorado weather and the choice and quality control of the solar monitoring sites. Funding was provided by DOE award DE-EE0002055.

Appendix: PV power production vs. load

Another important consideration of solar energy is how the power produced will correspond to the load. DOE electric energy use data for the state of Colorado for 2007 shows that Colorado's net generation was 53,907 GWh, or 1.94×10^{17} J [16]. The AVG4 site would have produced 6.4×10^{9} Wh m^{-2}. Considering a virtual solar array with a solar conversion efficiency of 0.15, we find that it would take roughly 2.0×10^{8} m^2 or about 77 mi^2 of PV panels to produce enough electricity for Colorado during 2007. For reference, a very large PV array at Nellis Air Force Base in Nevada covers only 0.22 mi^2 [17]. In addition to land requirements, a storage device that could store this amount of energy for up to 6 months would be required. It has been demonstrated for wind turbines that by using storage devices, such as compressed air, the capacity factor can be raised to a baseload level (greater than 70%) [18]. However, since the average PSD slope found in this study is flatter than for wind turbines, PV will likely require more supplementary storage than wind power.

These excessive land area and storage requirements show that it is very unlikely that solar power alone would ever power the entire state of Colorado, especially in the winter when evening heating demands are high and solar radiation is low. A better solution, at least in Colorado, appears to be using PV to supplement baseload power sources to cover the summer peak demand that is more synchronous with GHI [2,19].

References

[1] REN21: Renewables Global Status Report: 2009 Update; 2009:12.
[2] Sovacool BK. The intermittency of wind, solar, and renewable electricity generators: technical barrier or rhetorical excuse? Utilities Policy 2008;17:288–96.
[3] Kropp R. Solar expected to maintain its status as the world's fastest-growing energy technology. Sustainability Investment News; March 3, 2009.
[4] Beyer HG, Luther J, Steinberger-Willms R. Power fluctuations in spatially dispersed wind turbine systems. Solar Energy 1993;50:297–305.
[5] Focken U, Lange M, Monnich K, Waldl H, Beyer HG, Luig A. Short-term prediction. Journal of Wind Energy Engineering and Indstrial Aerodynamics 2002;90:231–46.
[6] Archer CL, Jacobson MZ. Supplying baseload power and reducing transmission requirements. Journal of Applied Meteorology and Climatology 2007;46:1701–17.
[7] Fgw, Iset. Increasing the penetration of wind energy in the European electricity network. Fordergesellschaft Windenergie. Institut fur Solar Energieversorgungstechnik; 2000. p. 47.
[8] Long CN, Ackerman TP. Surface measurements of solar irradiance: a study of the spatial correlation between simultaneous measurements at separated sites. Journal of Applied Meteorology 1995;34:1039–47.
[9] Barnett TP, Ritchie J, Stokes G. On the space-time scales of the surface solar radiation field. Journal of Climate 1998;11:88–96.
[10] Curtwright A, Apt J. The Character of power output from utility-scale photovoltaic systems. Progress in Photovoltaics 2008;16:241–7.
[11] Wiemken E, Beyer HG, Heydenreich W, Kiefer K. Power characteristics of PV ensembles: experiences from the combined power production of 100 grid connected PV systems distributed over the area of Germany. Solar Energy 2001;70(6):513–8.
[12] (NREL). N.R.E.L. Measurement and Instrumentation data Center (MIDC), http://www.nrel.gov/midc [accessed 04.11.09].
[13] Nanahara T, Asari M, Maejima T, Sato T, Yamaguchi K, Shibata M. Smoothing effects of distributed wind turbines. Part 2. Coherence among power output of distant wind turbines. Wind Energy 2004;7(2):75–85.
[14] Apt J. The spectrum of power from wind turbines. Journal of Power Sources 2007;169(2):369–74.
[15] Nanahara T, Asari M, Sato T, Yamaguchi K, Shibata M, Maejima T. Smoothing effects of distributed wind turbines. Part 1. Coherence and smoothing effects at a wind farm. Wind Energy 2004;7(2):61–74.
[16] DOE/EIA-0348(01)/2. Available at, http://www.eia.doe.gov/cneaf/electricity/st_profiles/colorado.html; April 2009 [accessed 04.11.09].
[17] Cnet News. Green Tech. Air force base in Nevada goes solar with 14-megawatt array. 5 December 2007. Available at, http://news.cnet.com/8301-11128_3-9829328-54.html [accessed 04.11.09].
[18] Denholm P, Kulcinski GL, Holloway T. Emissions and energy efficiency assessment of baseload wind energy systems. Environmental Science and Technolology 2005;39:1903–11.
[19] Denholm P, Margolis RM. Evaluating the limits of solar photovoltaics (PV) in traditional electric power systems. Energy Policy 2007;35:2853–61.